

Synergy in flame-retarded epoxy resin

Identification of chemical interactions by solid-state NMR

Aleksandra Sut¹ · Sebastian Greiser² · Christian Jäger² ·
Bernhard Schartel¹ 

Received: 22 June 2016 / Accepted: 26 October 2016 / Published online: 7 November 2016
© Akadémiai Kiadó, Budapest, Hungary 2016

Abstract The potential synergists aluminium diethylphosphinate (AlPi), boehmite (AlO(OH)) and melamine polyphosphate (MPP) were compared in flame-retardant epoxy resin (EP)/melamine poly(magnesium phosphate) (S600). The pyrolysis, the fire behaviour as well as the chemical interactions in the gas and condensed phases were investigated by various methods. Flammability was investigated by cone calorimeter and oxygen index (OI). The thermal and thermo-oxidative decomposition were studied by thermogravimetric analysis coupled with FTIR spectrometer. The special focus was on the investigation of structural changes in the condensed phase via solid-state NMR of ²⁷Al and ³¹P nuclei. By the comparison of epoxy resin with only one additive or with S600 in combination with AlPi, AlO(OH) or MPP, it was possible to calculate the synergy index. The best performance in terms of fire behaviour was observed for EP/S600/MPP with a PHRR (peak heat release rate) of 208 kW m⁻² due to slight synergy. In the case of THE (total heat evolved), clear synergy occurred for EP/S600/AlPi and EP/S600/AlO(OH). By solid-state NMR, different phosphates and aluminates were identified, indicating the chemical interactions between S600 and AlPi, AlO(OH) or MPP. The systematic multi-methodical approach yielded insight into the synergistic effects in the flame-retarded epoxy resin.

Keywords Synergy · Epoxy resin · Flame retardancy · Melamine poly(magnesium phosphate) · Solid-state NMR

Introduction

Epoxy resins are an important materials used in various applications due to their advantages like chemical resistance, good electrical properties and mechanical stability [1–3]. However, as they are based on hydrocarbon chains, in the case of fire the performance of many epoxy resins is rather poor, with fast burning and no residue formation. Nowadays compliance with fire-protection requirements is demanded for many applications, especially in electrical engineering and the transportation sector. At the same time, the market demands halogen-free flame retardants due to environmental aspects. To achieve suitable fire properties multi-component, synergistic systems are often used [4–10]. One of the approaches focuses on the specific condensed-phase reaction to achieve better flame retardancy [11]. Among many non-halogenated flame retardants, two groups of additives play the most important role: phosphorus-based additives and additives containing nitrogen. The special focus is on melamine polyphosphate (MPP), which combines the benefits of phosphorus with those of melamine [12, 13]. Moreover, MPP is often additionally modified to improve performance. Recently, a new group of melamine poly(metal phosphate) additives was introduced to the market under the brand name Safire [14–18].

In work presented, three multi-component systems were compared: epoxy resin (EP)/melamine poly(magnesium phosphate) (S600)/aluminium diethylphosphinate (AlPi), EP/S600/boehmite (AlO(OH)) and EP/S600/melamine polyphosphate (MPP), not only in terms of performance

✉ Bernhard Schartel
bernhard.schartel@bam.de

¹ Bundesanstalt für Materialforschung und –prüfung (BAM),
Unter den Eichen 87, 12205 Berlin, Germany

² Bundesanstalt für Materialforschung und –prüfung (BAM),
Richard-Willstätter-Str. 11, 12489 Berlin, Germany

and synergy to find the best formulation for epoxy resin, but also to understand the chemical processes in order to find promising approaches to synergy. A comprehensive, detailed and multi-method approach was used to study the chemical interactions occurring between the synergists.

Experimental

Materials

Bisphenol A diglycidyl ether (DGEBA, Araldite MY740, Bodo Möller Chemie GmbH, Offenbach, Germany) was mixed with isophorone diamine (IPDA, Merck KGaA, Darmstadt, Germany) and flame retardants in a glass beaker using a mechanical stirrer as described for similar compounds [19]. The total load of the additives was always 20 mass%. After mixing, the material was put in the aluminium trays to prepare the specimens. The curing process followed in three steps: 30 min at 80 °C, 30 min at 110 °C and 60 min at 160 °C. Afterwards, epoxy mixtures were cooled down to room temperature slowly in order to avoid cracking and then cut to the desired size. The following flame retardants were used: melamine poly(magnesium phosphate) (Safire® 600, Floridienne Chemie, Ath, Belgium), aluminium diethylphosphinate (Exolit OP 935, Clariant Produkte, Germany), boehmite (Apyral AOH 30, Nabaltec AG, Schwandorf, Germany) and melamine polyphosphate (Melapur 200 70, BASF SE, Ludwigshafen, Germany). The list of all materials investigated is presented in Table 1.

Methods

The fire behaviour under forced-flaming conditions was investigated using a cone calorimeter (Fire Testing Technology, East Grinstead, UK) according to ISO 5660. All specimens (100 × 100 × 3 mm) were conditioned for

48 h (23 °C, 50% relative humidity). Specimens were exposed to irradiation of 50 kW m⁻² with a distance of 35 mm between the surface and the cone heater. As investigated before, the distance of 35 mm provides homogenous irradiance of the inner area [20]. In order to prevent buckling of the samples before ignition, specimens were placed in retainer frame and an additional thin wire cross was used. Because the edges under the frame underwent combustion as well, the results were recalculated to 100 cm² surface area. The total heat evolved (THE) was declared to be the total heat released at the point where the smoke production was below 0.01 m² s⁻¹. These criteria had to be adopted as it was difficult to determine flameout due to the strong intumescence of some of the materials. No third measurement was taken when the deviation between the two first cone calorimeter measurements was less than 10% in all characteristics, so that evaluating two measurements deliver reliable results in accordance with the standard already. Reaction to a small flame (flammability) was determined by the limiting oxygen index (LOI) according to ISO 4589 (sample size 100 × 6.5 × 3 mm). All specimens were conditioned at 23 °C and 50% relative humidity for 48 h before the test.

Thermogravimetric analysis (TG) was performed on the TG 209 F1 Iris (Netzsch Instruments, Selb, Germany) coupled with a Fourier transform infrared spectrometer (FTIR, Tensor 27, Bruker Optics, Ettlingen, Germany) using a transfer line heated up to 260 °C in order to analyse the evolved gases. The temperature was chosen to detect the decomposition products of AlPi [21]. The materials were milled under liquid nitrogen in a CryoMill (RETSCH, Germany), and 5 mg of each material was measured in a crucible under nitrogen and synthetic air flow (30 mL min⁻¹) at a heating rate of 10 K min⁻¹.

Solid-state nuclear magnetic resonance (NMR) measurements were taken using an AVANCE 600 (14.1 T) spectrometer (Bruker Biospin GmbH, Rheinstetten, Germany) equipped with a wide-bore magnet. All experiments

Table 1 Composition of tested materials and corresponding abbreviations

Name	Acronym
DGEBA + IPDA	EP
EP + 20 mass% melamine poly(magnesium phosphate)	EP/S600
EP + 20 mass% aluminium diethylphosphinate (AlPi)	EP/AlPi
EP + 20 mass% boehmite (AIO(OH))	EP/AIO(OH)
EP + 20 mass% melamine polyphosphate (MPP)	EP/MPP
EP + 10 mass% S600 + 10 mass% AlPi	EP/S600/AlPi
EP + 10 mass% S600 + 10 mass% AIO(OH)	EP/S600/AIO(OH)
EP + 10 mass% S600 + 10 mass% MPP	EP/S600/MPP

were carried out at room temperature using the magic angle spinning technique (MAS). The fire residues were powdered using an agate mortar and packed up to the rotors (zirconia, Kel-F caps). The parameters of the measurements are listed in Tables 2 and 3. In case of ^{27}Al MAS NMR, the pulse length listed in Table 2 corresponds to the selective 90° condition for quadrupolar nuclei. For ^{27}Al , that pulse length equals 1/3 of a liquid state 90° pulse.

Results and discussion

Fire behaviour

Figure 1 presents heat release rate (HRR) curves over time for EP, EP/S600, EP/X (where X: AlPi, AIO(OH) or MPP) and EP/S600/X (Fig. 1a–c) as well the comparison of all systems with two additives (Fig. 1d). The forced-flaming behaviour and the reaction to small flame for EP, EP/S600 and EP/X have been described in detail before [19]. The shape of the HRR curve of EP indicates a non-charring sample of medium thickness [22, 23] with an additional peak near flameout. The first peak represents the peak heat release rate (PHRR), whereas a second minor maximum was caused by using the retainer frame. Initially, the edges of the sample were covered, but as combustion proceeded the material under the frame burned as well. EP shows a high PHRR of 1068 kW m^{-2} and forms no residue (Table 4). Adding the flame retardants reduced the PHRR, THE and THE/TML (TML = total mass loss). The time to ignition (t_{ig}) was slightly reduced for all flame-retarded formulations, suggesting that decomposition started at lower temperatures and/or that the viscosity of the material was changed [24]. For EP/S600, the PHRR decreased by more than 70% to 298 kW m^{-2} . A slight reduction in the THE/TML ratio was caused by the release of inert gases (e.g. ammonia); however, the difference was so low that it was concluded that S600 works mainly in the condensed phase and neither by fuel dilution nor by flame inhibition. In contrast, in the systems with AlPi THE/TML ratio was significantly reduced to 1.9 and $1.8 \text{ MJ m}^{-2} \text{ g}^{-1}$ for EP/AlPi and EP/AlPi/S600, respectively. It is known from the literature that the main mode of action of AlPi in many

systems is flame inhibition by evolving phosphorus species into the gas phase [21, 25–30]. Moreover, the LOI increased from 21.0 to 30.4% for EP/S600/AlPi compared to EP (Table 4). Thus, the performance for reaction to small flame test is improved, making it the best of all investigated materials. In cone calorimeter test, the reduction in PHRR was not so strong and similar for EP/AlPi and EP/S600/AlPi, yet lower PHRR was achieved for EP/S600. Therefore, when PHRR is considered, the materials are ranked as follows: EP > EP/AlPi \approx EP/S600/AlPi > EP/S600. In conclusion, the combination of AlPi and S600 did not change performance when compared to EP/AlPi in the cone calorimeter.

The worst performance of the flame-retarded formulations was observed for EP/AIO(OH). The shape of the HRR curve was same as for pure EP, but the peak was reached earlier. When AIO(OH) was combined with S600, the PHRR was reduced by almost half compared to EP/AIO(OH). In LOI test, an increase to 28.9% was achieved and stronger residue formation was observed than in EP/S600/AlPi and EP/S600/MPP. Taking into account the minor influence on the effective heat of combustion as well, it was concluded that the main mode of action of AIO(OH) is increased residue formation. As the residue formed did not provide a sufficient protection layer, the performance in cone calorimeter was worse than for other investigated materials. Since the result was better for EP/S600/AIO(OH) than for EP/AIO(OH), it suggests that S600 works not only by residue formation but also as a char stabilizer. Nevertheless, as for systems with AlPi, the best result was achieved for EP/S600.

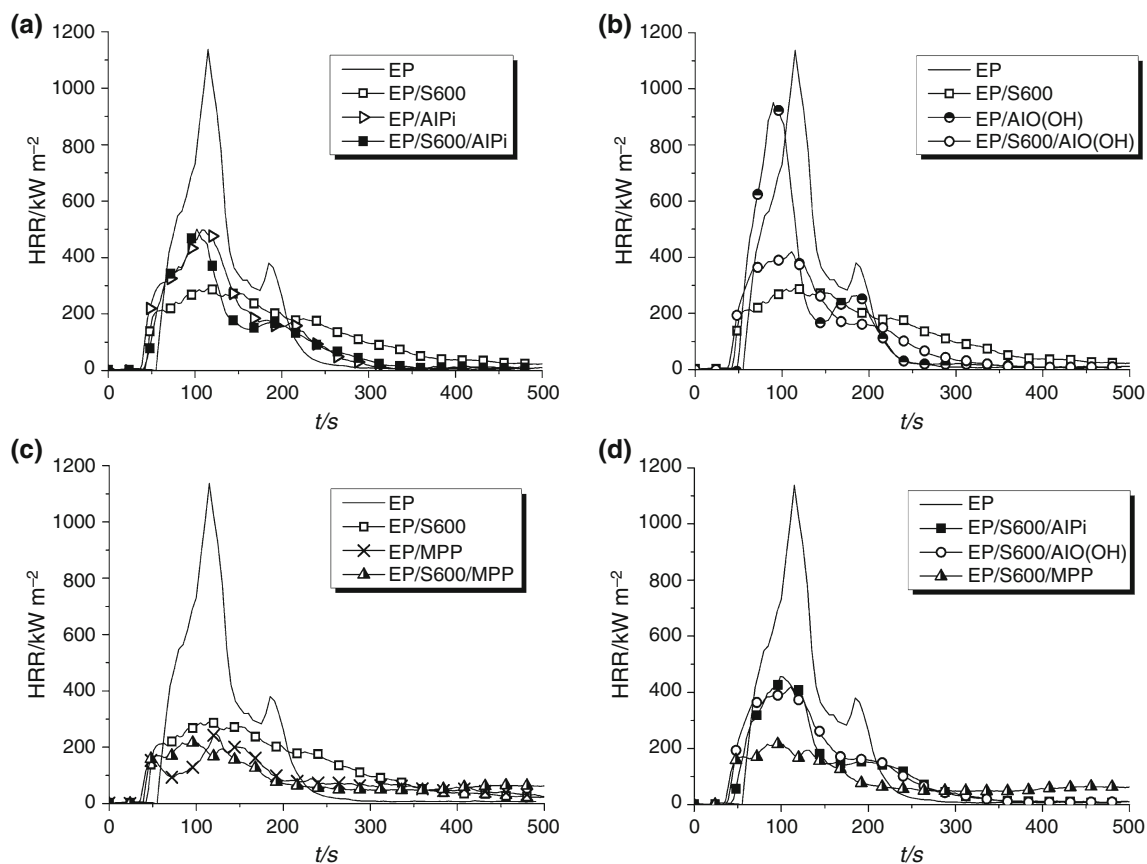
The strongest reduction in PHRR was observed when MPP was added to the epoxy system. MPP is known to cause intumescent effects; indeed, for both EP/MPP and EP/S600/MPP increased residue formation was observed, which worked as an insulation barrier. Similar to formulations with AIO(OH), the main effect was observed in the condensed phase by formation of an intumescent protective layer, which led to decreasing PHRR to 208 kW m^{-2} for EP/S600/MPP. In terms of PHRR, the materials are ranked as follows: EP > EP/S600 > EP/MPP > EP/S600/MPP and show clearly that the combination of both additives, MPP and S600, leads to the best performance.

Table 2 ^{27}Al MAS NMR parameters: DI—repetition time, P—pulse length, NS—number of scans

Name	DI/s	P/ μs	NS	Rotor/mm	Spinning speed/kHz
EP/AlPi; EP/S600/AlPi	2	2.25	128	4	12.5
EP/AIO(OH)	2	1.75	128	2.5	25
EP/S600/AIO(OH)	30	2.25	16	4	12.5

Table 3 ^{31}P MAS NMR parameters: $D1$ —repetition time, P —pulse length, NS —number of scans

Name	$D1/s$	$P/\mu\text{s}$	NS	Rotor/mm	Spinning speed/kHz
EP/S600; EP/S600/AIPi	2000	4.3	8	4	12.5
EP/AIPi; EP/S600/AIO(OH); EP/S600/MPP	300	4.3	8	4	12.5
EP/MPP	300	4.3	16	4	12.5

**Fig. 1** Heat release rate (HRR) of the EP, EP/S600 and compositions with: AIPi (a), AIO(OH) (b), MPP (c) and the comparison of epoxy systems with S600 in combination with AIPi, AIO(OH) or MPP (d)**Table 4** Cone calorimeter data: PHRR—peak of heat release, THE—total heat evolved, TML—total mass loss, t_{ig} —time to ignition

Name	t_{ig}/s	PHRR/ kW m^{-2}	THE/ MJ m^{-2}	THE/TML/ $\text{MJ m}^{-2} \text{g}^{-1}$	Residue/mass%	LOI
EP [19]	54 ± 4	1068 ± 8	76 ± 4	2.4	0	21.0 [31]
EP/S600 [19]	44 ± 4	298 ± 8	57 ± 4	2.2	10	—
EP/AIPi [19]	41 ± 4	492 ± 8	56 ± 4	1.9	13	—
EP/S600/AIPi	44 ± 2	479 ± 22	46 ± 3	1.8	9	30.4
EP/AIO(OH) [19]	49 ± 4	870 ± 8	65 ± 4	2.4	15	—
EP/S600/AIO(OH)	38 ± 2	437 ± 18	55 ± 2	2.2	16	28.9
EP/MPP [19]	38 ± 4	244 ± 8	26 ± 4	—	—	—
EP/S600/MPP	39 ± 3	208 ± 9	54 ± 2	2.2	18	28.4

Figure 1d presents the comparison of HRR curves for EP/S600/AIPi, EP/S600/AIO(OH) and EP/S600/MPP. AIPi and AIO(OH) do not differ much in their HRR curves despite their different modes of action, and EP/S600/MPP has the best overall performance in terms of fire behaviour. The residues after cone calorimeter testing of those systems are presented in Fig. 2. For EP/S600/AIPi and EP/S600/AIO(OH), the residue formed was very brittle and loose, whereas the residue of EP/S600/MPP formed an intumescent layer caused by the presence of MPP and had a closed surface.

Based on the cone calorimeter data, different kinds of action were distinguished depending on the synergist used (AIPi, AIO(OH) or MPP). EP/S600/AIPi showed a clear flame inhibition effect, indicated by a very low THE/TML ratio ($1.8 \text{ MJ m}^{-2} \text{ g}^{-1}$). For EP/S600/AIO(OH), an increase in char formation was observed; however, as it did not provide sufficient insulation, the PHRR was still high. In the case of EP/S600/MPP, too, increased char formation was observed (18 mass%), but the structure of the residue (porous and with a closed surface) led to better insulation properties and a decrease in PHRR to 208 kW m^{-2} .

To identify whether synergistic effects occur in the investigated materials, the synergy index was calculated according to Eq. 1, where Y was PHRR or THE, and x the percentage amount of the additive in the flame-retarded systems. Synergy is defined as an effect of two or more additives that is greater than the predicted sum of the effects of additives independently (superposition) [32]. All calculated synergy indexes are presented in Table 5. Depending on the SE, synergy ($SE > 1$), superposition ($SE = 1$) or an antagonistic effect ($SE < 1$) was defined.

$$SE_Y = \frac{Y_{EP} - Y_{EP+(FR1+FR2)}}{\frac{x_{FR1}}{x_{FR1}+x_{FR2}} \cdot (Y_{EP} - Y_{EP+FR1}) + \frac{x_{FR2}}{x_{FR1}+x_{FR2}} \cdot (Y_{EP} - Y_{EP+FR2})} \quad (1)$$

In the case of PHRR, a slight antagonistic effect was observed for EP/S600/AIPi and the PHRR was higher than for EP/S600 (Table 2). For EP/S600/AIO(OH), synergy was observed and a strong reduction in PHRR compared to EP/AI(OH) occurred; however, EP/S600 still presented better performance. In the case of EP/S600/MPP, synergy

Table 5 Synergy indexes calculated for PHRR and THE

Name	SE _{PHRR}	SE _{THE}
EP/S600/AIPi	0.9	1.5
EP/S600/AIO(OH)	1.3	1.4
EP/S600/MPP	1.1	0.6

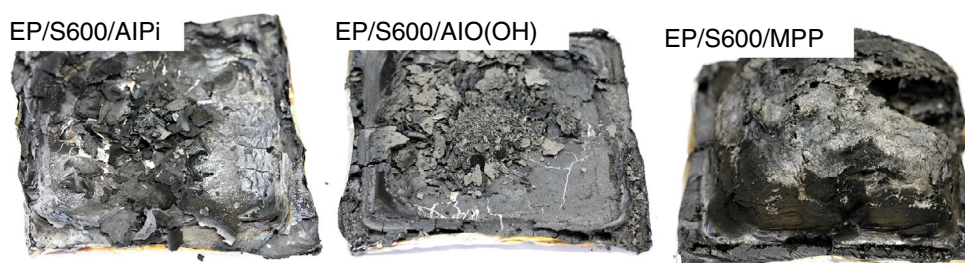
in PHRR was not as strong as in the case of EP/S600/AIO(OH), but it was concluded that with the same additive loading (20 mass%) a better result is achieved when S600 and MPP are combined than for single additive systems and that this improvement is more than superposition. In effect, the EP/S600/MPP system showed the best performance, with the lowest PHRR of 208 kW m^{-2} . It was proposed that the synergy and thus the best fire performance are the result of the superior combination of structural features of the fire residues of EP/MPP and EP/S600. EP/S600/MPP showed the closed surface and the increased height, but also an inner layered structure. Thus, the fire residue provided a highly effective protection layer. Similar observations were reported for epoxy resin flame retarded with melamine poly(zinc phosphate) and MPP [33].

When synergy in THE is considered, the results are different than for PHRR. The strongest synergy effect was observed for EP/S600/AIO(OH), but the resulting THE was the same as for EP/S600/MPP, even though it presented an antagonistic effect. Moreover, for EP/MPP the reduction of more than 50% in THE was observed when compared to EP/S600 or EP/S600/MPP. In the case of EP/S600/AIPi, strong synergy occurred as well, reducing the THE to 46 kW m^{-2} . This effect is due to the strong flame inhibition effect indicated by the low effective heat of combustion (expressed as THE/TML ratio).

Pyrolysis: mass loss and volatiles

In nitrogen atmosphere, decomposition occurred in a single step for all investigated materials (Fig. 3). All of the temperatures and corresponding mass losses are listed in Table 6. The temperature when 5 mass% mass loss was

Fig. 2 Fire residues of EP/S600/AIPi, EP/S600/AIO(OH) and EP/S600/MPP obtained in cone calorimeter



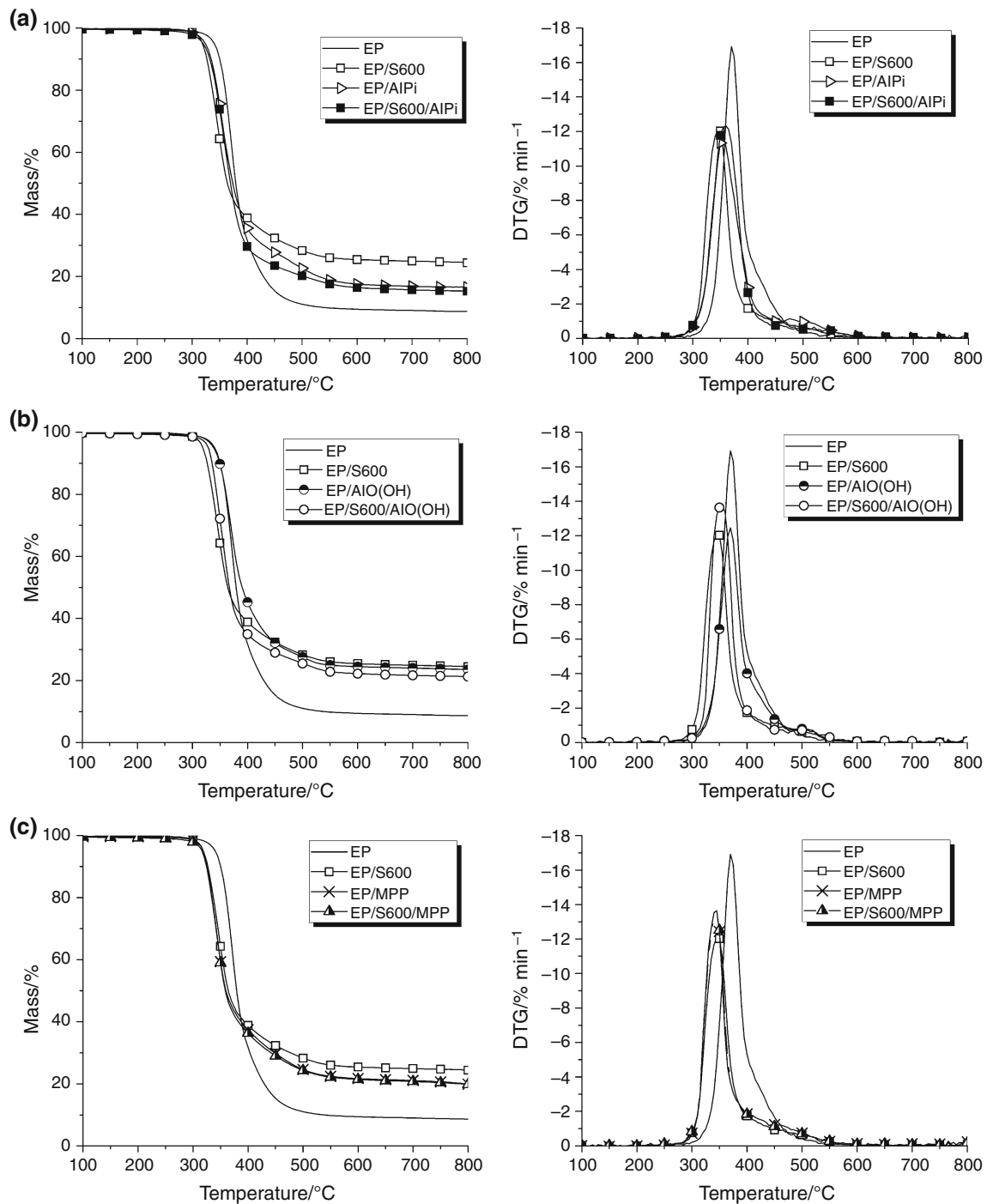


Fig. 3 Mass loss (TG) and mass loss rate (DTG) curves for epoxy resin systems with AIPi (a), AIO(OH) (b) and MPP (c) in the nitrogen atmosphere

observed ($T_{5\%}$) was taken as comparable measure for the beginning of decomposition. EP began decomposing at around 340 °C. When EP was mixed with additives, an evident shift towards lower temperatures was observed, except for EP/AIO(OH). This effect is attributed to two phenomena. First, the release of gases (e.g. ammonia, water) from the additives occurs at a lower temperature

than the decomposition of the EP, but the main reason for the shift is the interaction between the additives and the polymer matrix. The reduction in $T_{5\%}$ was not equal for the systems with additives. The lowest temperatures were observed for EP/S600, EP/MPP and EP/S600/MPP due to the strong interaction between the polymer and the melamine-based additive. It was observed that in PA6 the

Table 6 Thermal decomposition characteristics of the investigated materials in nitrogen atmosphere: $T_{5\%}$ —temperature for 5% mass loss; $T_{\max 1}$ —temperature of the maximum mass loss rate for first decomposition step; Δm_1 —mass loss at first decomposition step; residue mass taken at 800 °C

	EP	EP/S600	EP/AIPi	EP/S600/AIPi	EP/AIO(OH)	EP/S600/AIO(OH)	EP/MPP	EP/S600/MPP
$T_{5\%}/^{\circ}\text{C}$	340	320	324	320	339	329	319	317
$T_{\max 1}/^{\circ}\text{C}$	371	346	354	360	367	354	345	344
$\Delta m_1/\text{mass}\%$	91	75	83	83	76	70	79	78
Residue/mass% (at 800 °C)	9	24	16	15	23	21	20	20

presence of MPP led to a decrease in decomposition temperature due to the catalytic effect on amide scission, which led to strong Lewis acid–base interactions [13]. In EP/AIPi and EP/S600/AIPi, the $T_{5\%}$ was 16–20 °C lower than for EP, which suggests that AIPi has a weaker influence than MPP on the polymer matrix. Since AIO(OH) is an inert filler and does not interact with EP, the starting temperature was similar for EP/AIO(OH) (339 °C) and EP. When AIO(OH) was combined with S600, the temperature was lower but mainly due to the presence of S600.

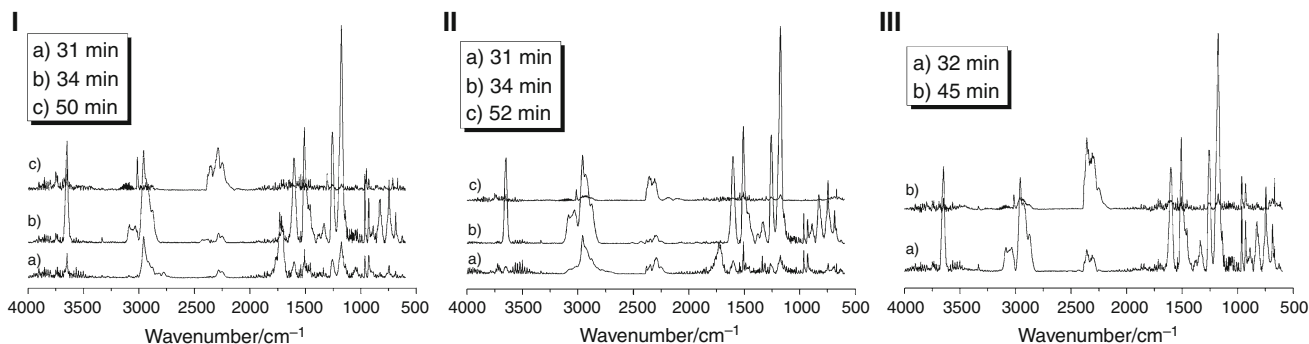
Moreover, it was observed that not only $T_{5\%}$ was shifted; the temperature of the maximum of the mass loss rate ($T_{\max 1}$) was also lower than for multi-component systems than for pure EP (Fig. 3). For EP, the maximum mass loss rate was at 371 °C and the mass loss was 91 mass%. The biggest shift clearly observed in Fig. 3 c was for EP/MPP, EP/S600 and EP/S600/MPP, with the temperature around 25 °C lower than for EP. There was no significant difference between EP/S600, EP/MPP and EP/S600/MPP in the decomposition process. The mass loss was around 78–79 mass% for EP/MPP and EP/S600/MPP and 75 mass% for EP/S600. A smaller change in $T_{\max 1}$ was observed in the cases of EP/AIPi and EP/S600/AIPi, which is consistent with previous observations suggesting an intermediate interaction with EP. The mass loss was higher than for systems with MPP due to the breaking of the P–C bond in AIPi and the partial release of phosphorus species into the gas phase. For EP/AIO(OH), the main decomposition step was shifted only slightly towards temperatures a

few degrees lower. In EP/S600/AIO(OH), the maximum of mass loss rate was at a lower temperature, which was caused by the presence of S600 in the system.

For all epoxy systems with additives, the final residue amount was close to 20 mass%, which stands for the load of additives in each system. This means that in all cases the additive contributed mainly by increasing the residue formation in the condensed phase. Nevertheless, the residues originate from different phenomena. For example, in the case of EP/AIO(OH) the residue was formed in the conversion process of AIO(OH) to Al_2O_3 . In EP/MPP, by contrast, the residue was an effect of increased char formation due to interaction between MPP and the polymer matrix.

In the systems with AIPi, the residue was lower than 20 mass% because of the partial decomposition of AIPi to the volatile products, acting as a flame inhibitor.

As observed in the TG, as mainly epoxy resin was decomposed, its decomposition products DGEBA/IPDA were expected to be found in the gas phase. Figure 4 presents FTIR spectra of EP/S600/AIPi, EP/S600/AIO(OH) and EP/S600/MPP, and they are consistent with the spectra of DGEBA/IPDA decomposition products reported in the literature [34–36]. In the cases of EP/S600/AIPi and EP/S600/AIO(OH), at first mainly C=O (1716 cm^{-1}), C–H (2779 cm^{-1}) and the trimethylamine group from IPDA (2958 cm^{-1}) were observed in the gas phase. The evolution of ammonia from S600 ($965, 930\text{ cm}^{-1}$) and a $\text{C}_{\text{Ar}}\text{--O}$ group in phenol ($1258, 1176\text{ cm}^{-1}$) also began. Subsequently,

**Fig. 4** FTIR spectra of the gas phase for EP/S600/AIPi (I), EP/S600/AIO(OH) (II) and EP/S600/MPP (III) in nitrogen atmosphere (31 min ≈ 344 °C, 32 min ≈ 354 °C, 34 min ≈ 372 °C, 45 min ≈ 485 °C, 50 min ≈ 534 °C, 52 min ≈ 556 °C)

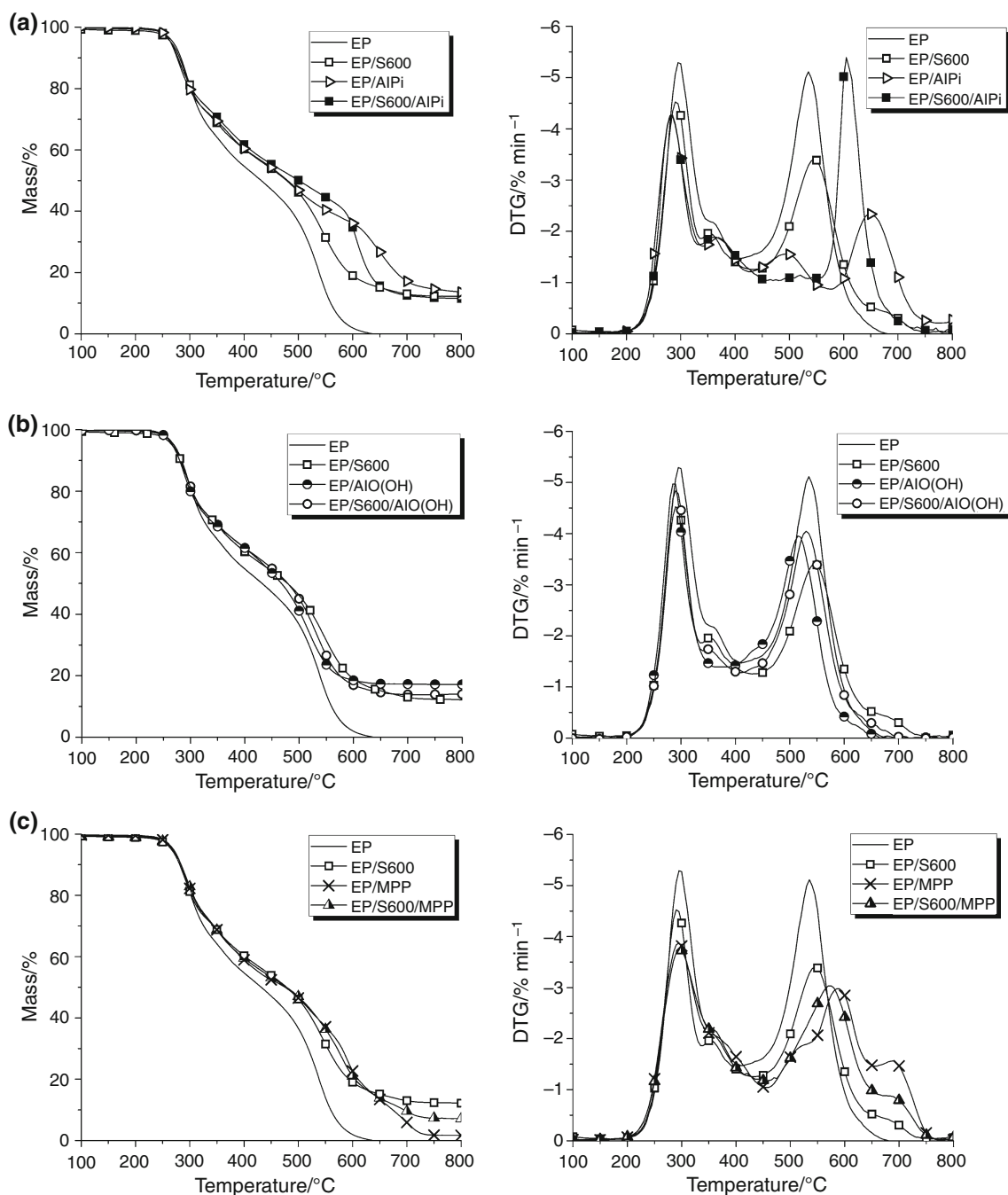


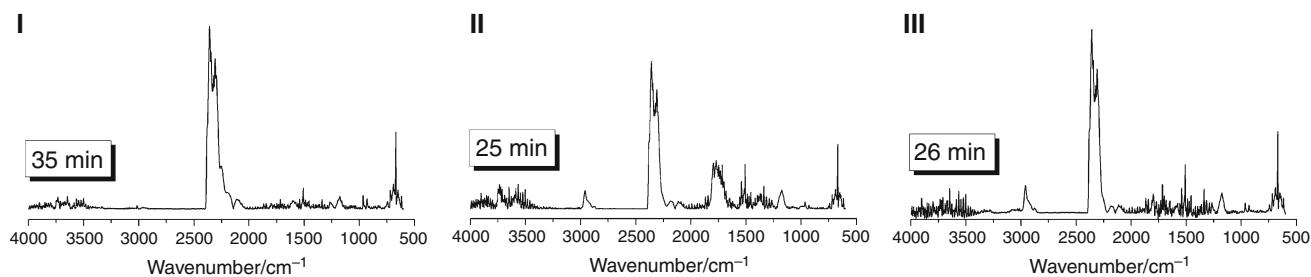
Fig. 5 Mass loss (TG) and mass loss rate (DTG) curves for epoxy resin systems with AlPi (a), AIO(OH) (b) and MPP (c) in synthetic air atmosphere

these signals became more intense and additional strong bands were also detected for $C_{Ar}=C_{Ar}$ ($1604, 1508\text{ cm}^{-1}$), OH-phenol groups of bisphenol A (3649 cm^{-1}) and $C_{Ar}-H$ ($3090-3030, 746, 686\text{ cm}^{-1}$). At the end of decomposition, mainly CO_2 ($2360-2250\text{ cm}^{-1}$) and methane (3015 cm^{-1}) were observed. In the case of EP/S600/AlPi, phosphorus species were expected to be present in the gas phase as well, but according to the mass loss observed in TG the release

was not high, so the intensity was lower and the signals were most probably overlapped by phenols. Based on results from TG-FTIR, it was concluded that in nitrogen atmosphere the additives result in increased residue formation and do not contribute significantly to the evolution of volatiles. In the case of EP/S600/MPP, no evident evolution of $C=O$ was observed, but the other signals were the same as for EP/S600/AlPi and EP/S600/AIO(OH).

Table 7 Thermo-oxidative decomposition characteristics of the investigated materials in synthetic air: $T_{5\%}$ —temperature for 5% mass loss; $T_{\max 1,2,3,4}$ —temperature of the maximum mass loss rate for first, second, third and fourth decomposition step; $\Delta m_{1,2,3,4}$ —mass loss at first, second, third and fourth decomposition step; residue mass taken at 800 °C

	EP	EP/S600	EP/AIPi	EP/S600/AIPi	EP/AIO(OH)	EP/S600/AIO(OH)	EP/MPP	EP/S600/MPP
$T_{5\%}/^{\circ}\text{C}$	270	266	265	265	267	269	296	269
$T_{\max 1}/^{\circ}\text{C}$	297	291	284	283	288	292	294	296
$\Delta m_1/\text{mass}\%$	48	44	29	27	36	29	48	48
$T_{\max 2}/^{\circ}\text{C}$	537	544	367	360	516	358	587	571
$\Delta m_2/\text{mass}\%$	51	42	13	29	46	17	39	35
$T_{\max 3}/^{\circ}\text{C}$	—	—	493	609	—	530	690	690
$\Delta m_3/\text{mass}\%$	—	—	19	32	—	39	13	8
$T_{\max 4}/^{\circ}\text{C}$	—	—	651	—	—	—	—	—
$\Delta m_4/\text{mass}\%$	—	—	24	—	—	—	—	—
Residue/mass% (at 800 °C)	0	12	14	11	17	14	2	7

**Fig. 6** FTIR spectra of the gas phase for EP/S600/AIPi (I), EP/S600/AIO(OH) (II) and EP/S600/MPP (III) in synthetic air atmosphere (25 min \approx 282 °C, 26 min \approx 292 °C, 35 min \approx 385 °C)

Thermo-oxidation: mass loss and volatiles

Thermo-oxidative decomposition was investigated by TG under synthetic air flow. Figure 5 presents the comparison of EP and EP in combination with one or two additives, with the temperatures for each decomposition step and the corresponding mass loss summarized in Table 7. EP and EP/S600 decompose in two main steps. On the DTG curve of EP, a small shoulder on the first peak was observed, but the difference was too small to be considered as an additional peak. The $T_{5\%}$ and $T_{\max 1}$ are decreased by few degrees for EP/S600, but the mass loss rate was slightly lower. At the second step, the mass loss was around 10 mass% lower for EP/S600 and yielded 12 mass% residue (at 800 °C), whereas for EP complete decomposition occurred with no residue remaining. In the systems with AIPi (Fig. 4a), the biggest differences from other systems were observed in the decomposition process. For EP/AIPi and EP/S600/AIPi, decomposition consisted of more steps and started few degrees earlier than for pure epoxy resin. The first decomposition step is similar whether or not AIPi is combined with S600, with the $T_{\max 1}$ at around 284 °C (13 °C lower than for EP) and a mass loss of 27–29 mass%. As the shoulder observed on the DTG curve

for EP became a separate peak in the cases of EP/AIPi and EP/S600/AIPi, it was considered to be an additional decomposition step with $T_{\max 2}$ of 360 and 367 °C for EP/AIPi and EP/S600/AIPi, respectively. Furthermore, EP/AIPi showed an additional step at around 493 °C, which was not observed in the case of EP/S600/AIPi. The last decomposition step was significantly shifted in the case of EP/AIPi to 651 °C, and the mass loss rate was much lower than for EP/S600/AIPi. These results suggest that S600 and AIPi interact with each other, but the residue formed is less thermally stable than in the case of systems with only one additive. This explains the fact that the amount of residue observed is lower than would be assumed by taking into account the contributions of the individual components.

In the cases of EP/AIO(OH) and EP/S600/AIO(OH) (Fig. 4b), no significant differences in temperatures are observed compared to EP and EP/S600, which is due to the fact that AIO(OH) is an inert filler and does not influence the decomposition behaviour of epoxy resin. Nevertheless, EP/AIO(OH) presents only two-step decomposition, with the residue yielding 17 mass%, attributed mainly to products of thermal conversion of AIO(OH) to Al_2O_3 . For EP/S600/AIO(OH), the decomposition is in three steps. The second step with $T_{\max 2}$ at 358 °C is, as in the case of AIPi

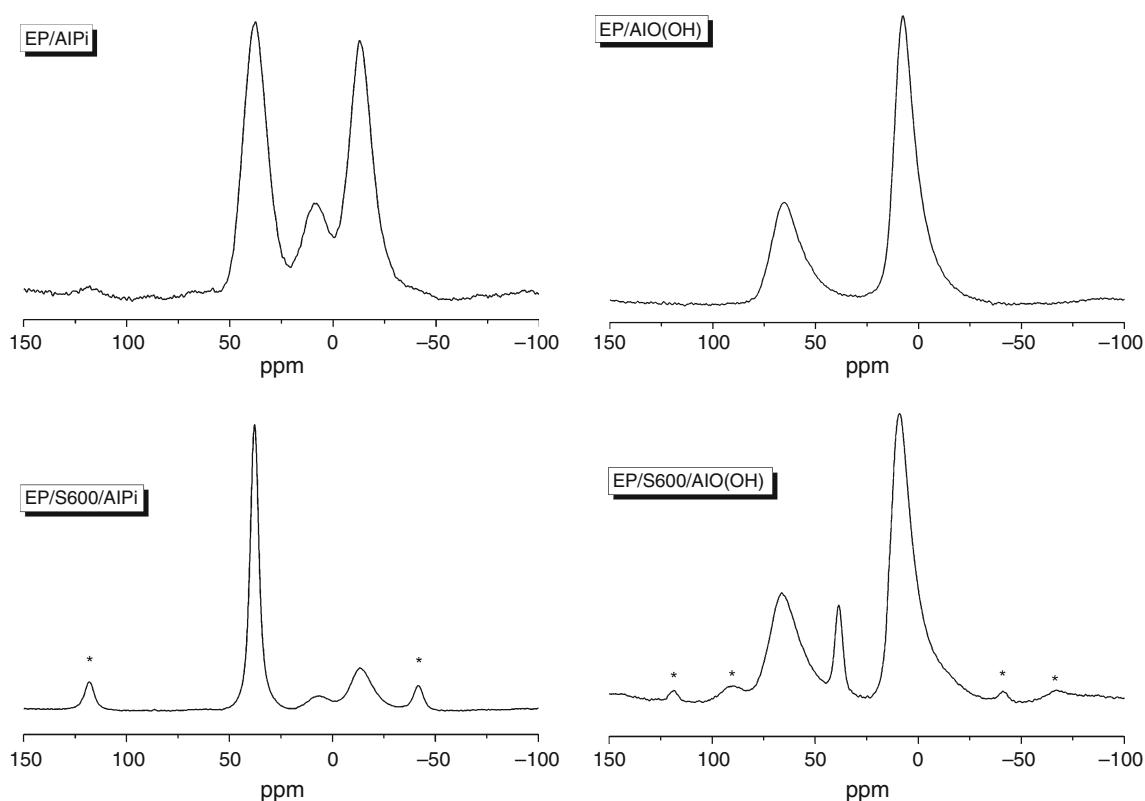


Fig. 7 ^{27}Al MAS NMR spectra for EP/AIPi, EP/S600/AIPi, EP/AIO(OH) and EP/S600/AIO(OH). Asterisks indicate spinning side bands

systems, considered to be an enhanced shoulder observed in EP. In the third decomposition step, the mass loss rate was the highest, yielding in 39 mass% mass loss. The residue remaining at 800 °C was 14 mass%, which might be considered as mostly inorganic residue formed in reaction of S600 with AIO(OH).

EP/MPP and EP/S600/MPP presented the lowest residue formation, in contrast to the results obtained in nitrogen atmosphere. Both combinations decomposed in three steps, decreasing the mass loss rate at each step compared to EP and EP/S600, but no thermally stable residue was formed. In the case of EP/S600/MPP, slightly more residue was left at 800 °C; nevertheless, the amount of the residue corresponds to the residue expected from the contributions of the individual components (around 7 mass%).

FTIR spectra of the gas phase are shown in Fig. 6. The main products observed in the gas phase for all tested materials were CO_2 (3735, 2359–2310, 669 cm^{-1}) and CO (2185, 2114 cm^{-1}), as expected. Nevertheless, other signals were also observed. For EP/S600/AIPi, EP/S600/AIO(OH) and EP/S600/MPP, similar as in the nitrogen atmosphere, the signals for ammonia were observed (965, 930 cm^{-1}). $\text{C}_{\text{Ar}}=\text{C}_{\text{Ar}}$ and $\text{C}_{\text{Ar}}-\text{O}$ were identified as well (bands at 1508 and 1176 cm^{-1}). In the cases of EP/S600/AIO(OH) and EP/S600/MPP, a clear signal for alkyl amines was detected, whereas for EP/S600/AIPi it was absent.

Moreover, only for EP/S600/AIO(OH) a strong signal for the C=O bond of carbonyl derivatives was observed (1771 cm^{-1}).

Analysis of the condensed phase: solid-state NMR

The fire residues remaining after the cone calorimeter test were analysed by solid-state NMR in order to identify the inorganic residue formed during the burning process. ^{27}Al MAS NMR for EP/AIPi, EP/S600/AIPi, EP/AIO(OH) and EP/S600/AIO(OH) are presented in Fig. 7.

The spectrum of EP/AIPi presents typical signals coming from the AIPi conversion. The resonances at around 38, 7.5 and -13.5 ppm were assigned to $[\text{AlO}_4]$, $[\text{AlO}_5]$ and $[\text{AlO}_6]$ units, respectively, and they formed a rather amorphous structure. Moreover, the chemical shift of $[\text{AlO}_4]$ units is typical for an AlPO_4 structure [27, 37]. When AIPi was combined with S600, this signal became stronger and narrower, suggesting the formation of more crystalline species. In the case of EP/AIO(OH), two signals were observed at 9.5 ppm and around 66 ppm and were attributed to octahedral and tetrahedral coordination in Al_2O_3 [38], which is a product of the dehydration of AIO(OH) structures at high temperatures. For EP/S600/AIO(OH), a new signal appeared at 38 ppm as the formation of AlPO_4 occurred. According to this result, it was

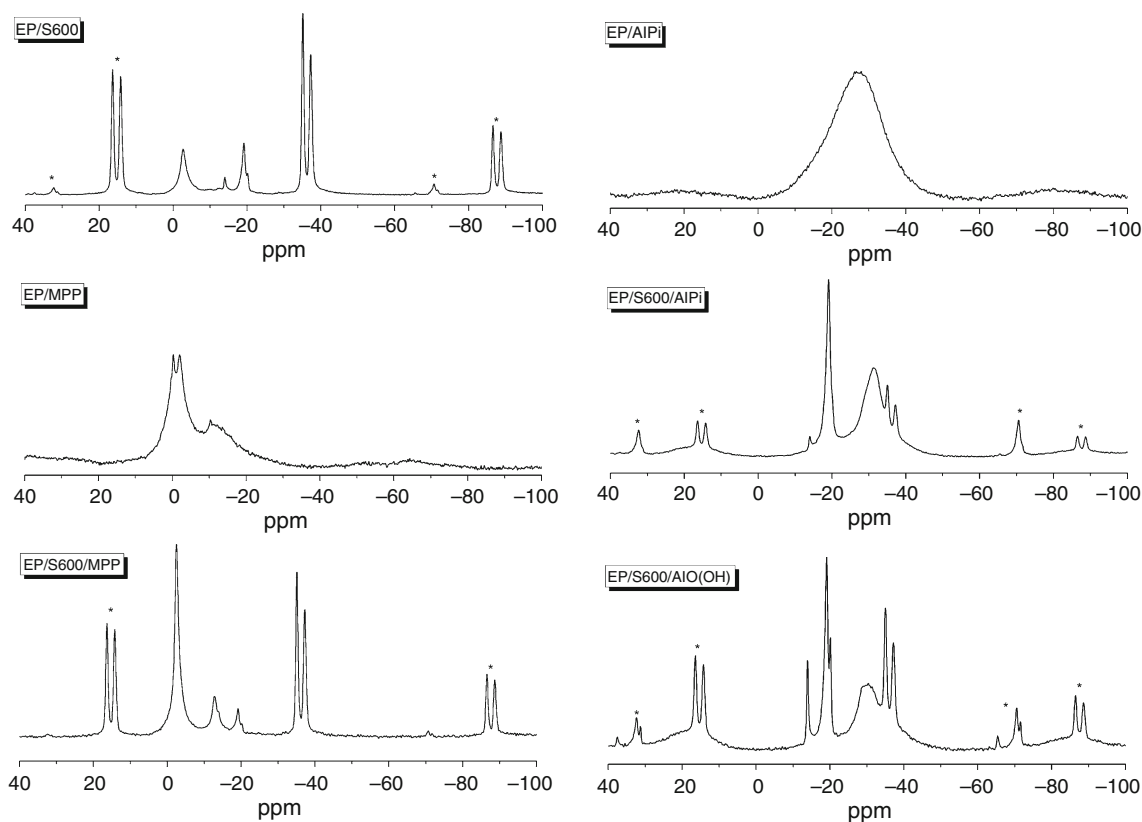


Fig. 8 ^{31}P MAS NMR spectra for EP/S600, EP/MPP, EP/AlPi, EP/S600/MPP, EP/S600/AlPi and EP/S600/AlO(OH). Asterisks indicate spinning side bands

concluded that most of the AlO(OH) was converted to aluminium oxide and some of the aluminium phosphate was formed as a product of the chemical interaction between S600 and AlO(OH).

Figure 8 presents ^{31}P MAS NMR of the residues for the epoxy system with one or two additives. In the EP/S600 spectrum, multiple signals are observed, corresponding to the decomposition products of S600, like magnesium orthophosphate (-2.5 ppm) and pyrophosphate (-14 , -19 ppm). Moreover, strong signal of crystalline structures was detected at -35 and -37 ppm, assigned to magnesium phosphate, and the chemical shift suggests the chain and/or ring formation [39, 40]. The shapes of the resonances indicate the differences in the degree of crystallinity—the narrower the signal, the more ordered (crystalline) the structure. In the case of EP/MPP, as reported before, mostly amorphous pyrophosphates and slightly crystalline melamine phosphate (around 0 ppm) remained in the residue as the products of the depolymerisation of MPP and interaction with the epoxy resin [33, 41]. When both of additives were combined in EP/S600/MPP, the signals observed for S600 were present in the spectrum as well, but additional strong, highly crystallized orthophosphate was also formed (around 0 ppm),

and the broad signal observed in the spectrum of EP/MPP vanished. This suggests that the interaction between the two additives leads to the formation of crystalline magnesium orthophosphate, which is dominant.

For EP/AlPi, only one signal is observed around -30 ppm, assigned to the AlPO_4 -type amorphous structures, a typical product of the thermal treatment of AlPi, and corresponds to the signal around -38 ppm observed in the ^{27}Al MAS NMR spectrum. The signal observed in the spectrum was very broad and suggested high disorder in the formed structure. When compared to our previous work, where AlPi was used in the TPE-S, it was concluded that the decomposition process of AlPi depends on the system in which it is used [37]. In the case of EP/S600/AlPi, this signal was still observed; however, crystalline magnesium pyrophosphate was dominant. Additional signals are present at -35 and -37 ppm as well as a minor signal at around -18 ppm coming from magnesium phosphate. A similar observation was made for EP/S600/AlO(OH), but the relative intensities were different. While for EP/S600/AlPi AlPO_4 might be formed from transformation of AlPi as well as from interaction between AlPi and S600, in the case of EP/S600/AlO(OH), it was a product of chemical interaction between S600 and AlO(OH).

Conclusions

In the presented work, three different potential synergists for melamine poly(magnesium phosphate)—AlPi, AlO(OH) and MPP—were investigated in terms of their influence on the fire behaviour and chemistry in the gas and the condensed phases. The best performance under forced-flaming conditions (cone calorimeter) was found for the EP/S600/MPP system; however, in the case of reaction to small flame, the best results were obtained for EP/S600/AlPi. By additional investigation of EP with only one additive, it was possible to calculate the synergy indexes. Depending on the parameter (PHRR or THE), synergy was found for each epoxy system with two additives, and the strongest synergistic effect was observed in THE for EP/S600/AlPi. By investigating the residues with the use of solid-state NMR, the chemical interactions between the additives were studied. Chemical interactions between AlO(OH) and S600 were indicated by formation of aluminium phosphate, whereas for other systems the products indicated in the condensed phase are also formed in the EP with only one additive. The multi-method approach used in this study allowed not only to identify the synergistic effects, but also to understand the chemical processes behind it.

Acknowledgements The authors would like to say special thanks to Tobias Kukofka for LOI measurements, to Patrick Müller and Thomas Rybak for help with the sample preparation and to Patrick Klack for technical support.

References

- Lee H, Neville K. Handbook of epoxy resins. New York: McGraw-Hill; 1982.
- Ellis B. Chemistry and technology of epoxy resins. Chemistry and technology of epoxy resins. London: Blackie Academic & Professional; 1993.
- Pham HQ, Marks MJ. Epoxy resins. In: Kirk RE, Othmer DF, Kroschwitz JI, Howe-Grant M, editors. Kirk-othmer encyclopedia of chemical technology. New York: Wiley; 1991.
- Wawrzyn E, Scharrel B, Karrasch A, Jäger C. Flame-retarded bisphenol a polycarbonate/silicon rubber/bisphenol a bis(diphenyl phosphate): adding inorganic additives. *Polym Degrad Stab*. 2014;106:74–87.
- Despinasse M-C, Scharrel B. Aryl phosphate-aryl phosphate synergy in flame-retarded bisphenol a polycarbonate/acrylonitrile-butadiene-styrene. *Thermochim Acta*. 2013;563:51–61.
- Despinasse M-C, Scharrel B. Influence of the structure of aryl phosphates on the flame retardancy of polycarbonate/acrylonitrile-butadiene-styrene. *Polym Degrad Stab*. 2012;97:2571–80.
- Langfeld K, Wilke A, Sut A, Greiser S, Ulmer B, Andrievici V, et al. Halogen-free fire retardant styrene-ethylene-butylene-styrene-based thermoplastic elastomers using synergistic aluminium diethylphosphinate-based combinations. *J Fire Sci*. 2015;33:157–77.
- Wang Y, Zhang L, Yang Y, Cai X. Synergistic flame retardant effects and mechanisms of aluminum diethylphosphinate (AlPi) in combination with aluminum trihydrate (ATH) in UPR. *J Therm Anal Calorim*. 2016;125:839–48.
- Zhang F, Chen P, Wang Y, Li S. Smoke suppression and synergistic flame retardancy properties of zinc borate and diantimony trioxide in epoxy-based intumescent fire-retardant coating. *J Therm Anal Calorim*. 2016;123:1319–27.
- Zhang L, Wang Y, Liu Q, Cai X. Synergistic effects between silicon-containing flame retardant and DOPO on flame retardancy of epoxy resins. *J Therm Anal Calorim*. 2016;123(2):1343–50.
- Scharrel B, Perret B, Dittrich B, Ciesielski M, Krämer J, Müller P, et al. Flame retardancy of polymers: the role of specific reactions in the condensed phase. *Macromol Mater Eng*. 2016;301:9–35.
- Döring M, Ciesielski M, Heinzmann C. Synergistic flame retardant mixtures in epoxy resins. In: Morgan AB, Wilkie CA, Nelson GL, editors. Fire and polymers VI: new advances in flame retardant chemistry and science. Washington: ACS Symposium Series; 2012.
- Braun U, Scharrel B, Fichera MA, Jäger C. Flame retardancy mechanisms of aluminium phosphinate in combination with melamine polyphosphate and zinc borate in glass-fibre reinforced polyamide 6,6. *Polym Degrad Stab*. 2007;92(8):1528–45.
- Wehner W, Dave T. Inventors; phosphorhaltige triazinverbindungen als flammenschutzmittel. Germany; 2009.
- Köstler H-G, Wehner W. Inventors; flammenschutzmittelzusammensetzungen enthaltend triazin-interkalierte metall-phosphate. Germany; 2012.
- Naik A, Fontaine G, Samyn F, Delva X, Bourgeois Y, Bourbigot S. Melamine integrated metal phosphates as non-halogenated flame retardants: synergism with aluminium phosphinate for flame retardancy in glass fiber reinforced polyamide 66. *Polym Degrad Stab*. 2013;98:2653–62.
- Naik A, Fontaine G, Samyn F, Delva X, Louisy J, Bellayer S, et al. Outlining the mechanism of flame retardancy in polyamide 66 blended with melamine-poly(zinc phosphate). *Fire Safety J*. 2014;70:46–60.
- Naik A, Fontaine G, Samyn F, Delva X, Louisy J, Bellayer S, et al. Mapping the multimodal action of melamine-poly(aluminium phosphate) in the flame retardancy of polyamide 66. *RCS Adv*. 2014;4:18406–18.
- Müller P, Scharrel B. Melamine poly(metal phosphates) as flame retardant in epoxy resin: performance, modes of action, and synergy. *J Appl Polym Sci*. 2016;133(24):43549.
- Scharrel B, Bartholmai M, Knoll U. Some comments on the use of cone calorimeter data. *Polym Degrad Stab*. 2005;88:540–7.
- Brehme S, Köppl T, Scharrel B, Altstädt V. Competition in aluminium phosphinate-based halogen-free flame retardancy of poly(butylene terephthalate) and its glass-fibre composites. *E Polym*. 2014;14(3):193–208.
- Scharrel B, Hull TR. Development of fire-retarded materials—interpretation of cone calorimeter data. *Fire Mater*. 2007;31:327–54.
- Scharrel B. Uses of Fire Tests in Materials Flammability Development. In: Wilkie CA, Morgan AB, editors. Fire retardancy of polymeric materials. Boca Raton: CRC Press; 2010. p. 421–51.
- Dittrich B, Wartig K-A, Hofmann D, Mülhaupt R, Scharrel B. Carbon black, multiwall carbon nanotubes, expanded graphite and functionalized graphene flame retarded polypropylene nanocomposites. *Polym Adv Technol*. 2013;24(10):916–26.
- Braun U, Bahr H, Sturm H, Scharrel B. Flame retardancy mechanisms of metal phosphinates and metal phosphinates in combination with melamine cyanurate in glass-fiber reinforced poly(1,4-butylene terephthalate): the influence of metal cation. *Polym Adv Technol*. 2008;19:680–92.

26. Braun U, ScharTEL B. Flame retardancy mechanisms of aluminium phosphinate in combination with melamine cyanurate in glass-fibre-reinforced poly(1,4-butylene terephthalate). *Macromol Mater Eng.* 2008;293:206–17.
27. Duquesne S, Fontaine G, Cerin-Delaval O, Gardelle B, Tricot G, Bourbigot S. Study of the thermal degradation of an aluminium phosphinate-aluminium trihydrate combination. *Thermochim Acta.* 2013;551:175–83.
28. Gallo E, Braun U, ScharTEL B, Russo P, Acierno D. Halogen-free flame retarded poly(butylene terephthalate) (PBT) using metal oxides/PBT nanocomposites in combination with aluminium phosphinate. *Polym Degrad Stab.* 2009;94(8):1245–53.
29. Gallo E, ScharTEL B, Braun U, Russo P, Acierno D. Fire retardant synergisms between nanometric Fe₂O₃ and aluminum phosphinate in poly(butylene terephthalate). *Polym Adv Technol.* 2011;22(12):2382–91.
30. Gallo E, ScharTEL B, Acierno D, Russo P. Flame retardant bio-composites: synergism between phosphinate and nanometric metal oxides. *Eur Polym J.* 2011;47(7):1390–401.
31. Täuber K, Marsico F, Wurm FR, ScharTEL B. Hyperbranched poly(phosphoester)s as flame retardants for technical and high performance polymers. *Polym Chem.* 2014;5:7042–53.
32. Weil ED. Additivity, synergism and antagonism in flame retardancy. In: Kuryla WC, Papa AJ, editors. *Flame retardancy of polymeric materials.* New York: Marcel Dekker; 1975. p. 185–243.
33. Müller P, Morys M, Sut A, Jäger C, Illerhaus B, ScharTEL B. Melamine poly(zinc phosphate) as flame retardant in epoxy resin: decomposition pathways, molecular mechanism and morphology of fire residues. *Polym Degrad Stab.* 2016;130:307–19.
34. Perret B, ScharTEL B, Stoss K, Ciesielski M, Diederichs J, Doring M, et al. A new halogen-free flame retardant based on 9,10-Dihydro-9-oxa-10-phosphaphenanthrene-10-oxide for epoxy resins and their carbon fiber composites for the automotive and aviation industries. *Macromol Mater Eng.* 2011;296(1):14–30.
35. Lee L-H. Mechanisms of thermal degradation of phenolic condensation polymers. II. Thermal stability and degradation schemes of epoxy resins. *J Polym Sci Part A.* 1965;3(3):859–82.
36. Levchik SV, Camino G, Luda MP, Costa L, Muller G, Costes B. Epoxy resins cured with aminophenylmethylphosphine oxide—II. Mechanism of thermal decomposition. *Polym Degrad Stab.* 1998;60(1):169–83.
37. Sut A, Greiser S, Jäger C, ScharTEL B. Interactions in multicomponent flame-retardant polymers: solid-state NMR identifying the chemistry behind it. *Polym Degrad Stab.* 2015;121:116–25.
38. Müller D, Gessner W, Samoson A, Lippmaa E, Scheler G. Solid-state ²⁷Al NMR studies on polycrystalline aluminates of the system CaO–Al₂O₃. *Polyhedron.* 1986;5:779–85.
39. Fichera MA, Braun U, ScharTEL B, Sturm H, Knoll U, Jäger C. Solid-state NMR investigations of the pyrolysis and thermo-oxidative decomposition products of a polystyrene/red phosphorus/magnesium hydroxide system. *J Anal Appl Pyrolysis.* 2007;78(2):378–86.
40. Fayon F, Massiot D, Suzuya K, Price DL. ³¹P NMR study of magnesium phosphate glasses. *J Non Cryst Solids.* 2001;283:88–94.
41. Jahromi S, Gabriëlse W, Braam A. Effect of melamine polyphosphate on thermal degradation of polyamides: a combined X-ray diffraction and solid-state NMR study. *Polymer.* 2003;44:25–37.